PCCP

PAPER

Cite this: *Phys. Chem. Chem. Phys.*, 2016, **18**, 8865

Structure and rheology of gel nanostructures from a vitamin C-based surfactant†

Emiliano Carretti,[a] Virginia Mazzini,[ab] Emiliano Fratini,[a] Moira Ambrosi,[a] Luigi Dei,[ac] Piero Baglioni[ac] and Pierandrea Lo Nostro*[ac]

Received 16th December 2015,
Accepted 1st March 2016

DOI: 10.1039/c5cp07792c

www.rsc.org/pccp

The structure and rheology behaviour of gels produced by water dispersions of a vitamin C-derived surfactant (ascorbyl-6-*O*-dodecanoate) were investigated by means of SAXS and rheology experiments for the first time. The gel state is formed upon heating and is due to an anisotropic expansion of the tightly compact lamellar structure. The phase transition involves primarily the melting of the alkyl chains and a significant increment in the interlamellar water layer. In particular, our results show that in the gel the hydrophobic chains are in a liquid-like state, as in the core of a micelle, while the head groups release their acidic proton, become negatively charged and determine the onset of strong electrostatic interactions between facing lamellae. The full hydration of the anionic head groups and the uptake of a significant amount of water increase the interlamellar thickness and stabilise the gel structure. Rheology and SAXS measurements together provide an updated picture for the gel state. Moreover, for the first time we show the presence of a concentration threshold, above which the self-assembled aggregates interact more strongly and deplete some of the water that is retained in the interlamellar region.

1 Introduction

The size, shape and properties of self-assembled nanostructures depend on the nature and composition of the amphiphilic building blocks. In particular, the charge and the hydrogen bonding capacity of their head groups, the extension of the lipophilic tails, the peculiar stereochemistry and rigidity of the backbone are the main structural factors that lead to the formation and determine the performances of a nanoaggregate. External factors such as temperature, concentration and addition of cosolutes (strong electrolytes or neutral molecules) contribute in setting the phase behaviour.[1,2] At the molecular and supramolecular levels, the construction of a nanostructure requires different kinds of non-covalent interactions that include van der Waals, hydrophobic, hydration, dipolar, and electrostatic forces.[2] Furthermore, the structure and functionalities of more complex nanoscaled biological systems such as biomembranes and cytoplasmic organelles are controlled by the same interactions. For this reason a deep study of surfactant-based self-assemblies is necessary in order to understand and control the nature and behaviour of higher hierarchical biostructures.

In previous works, we investigated the self-assembly properties of 6-*O*-ascorbyl-alkanoates in water and in organic solvents, and found that the structural features, hydration and phase behaviour of their nanostructures strictly depend on the peculiar properties of the ascorbic acid moiety: the presence of a quite rigid lactone ring, of a redox active group, of three hydroxyl groups that are available for hydrogen bonding and the presence of two stereogenic centres in positions 4 and 5 as depicted in Fig. 1 (see Borsacchi *et al.*[3] and references therein).

The self-assembly of ascorbyl-alkanoates in water has been studied through a variety of techniques, including conductivity, differential scanning calorimetry (DSC), surface tension, small angle X-ray scattering (SAXS), small-angle neutron scattering (SANS), cryo-transmission electron microscopy (cryo-TEM), and X-ray diffraction (XRD) experiments. In previous papers, we reported on the behaviour of single chained L-ascorbic acid

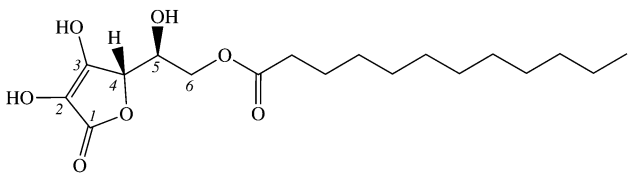

Fig. 1 [(2*S*)-2-[(2*R*)-4,5-Dihydroxy-3-oxo-2-furyl]-2-hydroxy-ethyl] dodecanoate (or ascorbyl dodecanoate, L-ASC12).

[a] *Department of Chemistry and CSGI, University of Florence, 50019 Sesto Fiorentino, Firenze, Italy. E-mail: PLN@csgi.unifi.it; Fax: +39 055 457 3010; Tel: +39 055 457 3036*

[b] *Department of Applied Mathematics, Research School of Physics and Engineering, The Australian National University, Canberra, ACT 0200, Australia*

[c] *Enzo Ferroni Foundation, 50019 Sesto Fiorentino, Firenze, Italy*

† Electronic supplementary information (ESI) available. See DOI: 10.1039/c5cp07792c

esters (L-ASC*n*, where *n* refers to the number of carbons in the hydrocarbon chain) in water at different pH and in the presence of salts and other solutes.[3–5]

More recently, we studied the self-assembly of a bolaamphiphile that carries two L-ascorbic acid moieties,[2] of a double chained derivative,[6] and of D-isoascorbic acid amphiphilic derivatives.[7] We found that changing the stereochemistry from L-ASC to D-isoASC brings about a significant variation in the hydration of the head groups, because of the different set of hydrogen bonding: L-ascorbic acid residues form several intermolecular bonds, while intramolecular interactions prevail in the D-isoascorbic moieties. This stereochemical feature determines different properties in the solid state and in solution.[7,8]

The phase behaviour of these surfactants' water dispersions include a transition from a coagel state to a gel phase that occurs upon heating and that is due to the collapse of the hydrated and tightly packed lamellar phase into a translucent, highly viscous phase, the gel, for $n > 10$ (see Fig. 2). For $n \leq 10$ instead a clear liquid micellar dispersion is formed.

The transition temperature depends on the number of carbons in the lipophilic tail, and does not significantly change when the surfactant mass fraction ranges between 5% and 50%. In the coagel state the aliphatic tails are arranged in compact layers with interdigitated chains and a low degree of tilting, while a thin layer (about 1 nm) of strongly bound water molecules separates the hydrophilic regions of two adjacent lamellae. Optical microscopy under crossed polarizers and environmental scanning electron microscope (ESEM) micrographs show the presence of extended highly oriented structures, similar to a house of cards, like those found in smectic liquid crystals.[5] As temperature increases above the transition point, the hydrophobic tails melt, the bulk free water disappears, and the surfactant lamellar layers are separated by a thicker water pool, that is usually referred to as intermediate water. Such a scheme parallels that proposed by for aqueous dispersions of quaternary ammonium amphiphiles.[9]

Although the occurrence and description of these phases are well-known and have been reported in several studies (see Borsacchi *et al.*[3] and references therein), the real meaning of terms such as gel and intermediate water need to be clarified. In a previous contribution we investigated the dynamic properties of the gel and coagel states, and the nature of the intermediate water, whose dynamic properties apparently derive from the merging between the strongly bound and the free bulk water molecules that are present in the coagel phase.[3]

In this paper we address the structure and rheology properties of the gel phase produced by L-ascorbyl-dodecanoate (L-ASC12) in water, as a function of mass fraction and temperature. The results indicate that, upon heating, the compact lamellar fully interdigitated structure of the coagel collapses, the alkyl chains acquire liquid-like behaviour and the hydrophilic pool becomes much wider.

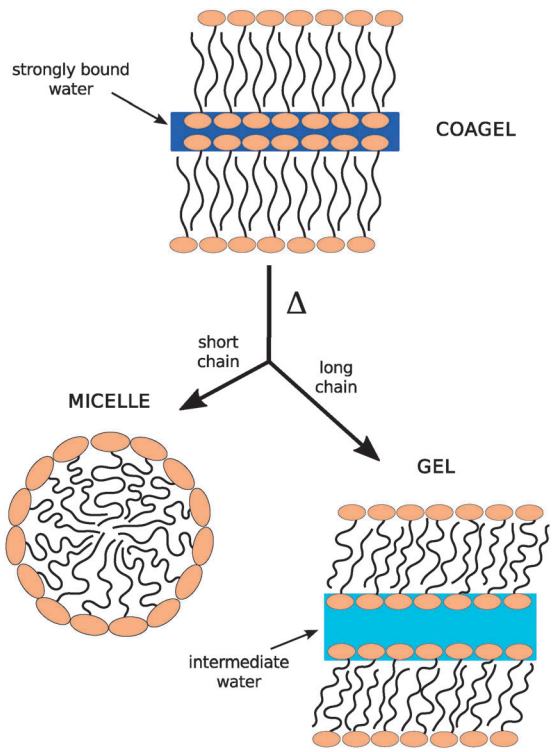

Fig. 2 Phase transitions for the L-ASC*n* system.

2 Experimental section

2.1 Synthesis of surfactant

L-ASC12 surfactant was synthesized according to the procedure reported in the literature.[10] Purity was controlled by TLC, elemental analysis and DSC.

2.2 Sample preparation

In order to obtain homogeneous samples, aqueous dispersions of L-ASC12 were treated according to a double annealing procedure. The first cycle was performed immediately after the mixing of L-ASC12 and water at 65 °C in a bath. In this step it is crucial to remove the air entrapped in the system. This feature is particularly important for the rheological measurements, in fact residual air bubbles could not be eliminated during the second annealing cycle, which is directly carried out on the rheometer plate according to the following sequence:

(1) isothermal treatment for 3 min at 60 °C
(2) cooling from 60 °C to 10 °C in 5 min
(3) heating from 10 °C to 60 °C in 5 min
(4) isothermal treatment for 10 min at 60 °C
(5) for the gel, cooling from 60 °C to the measurement temperature in 5 min, or for the coagel, cooling from 60 °C to 10 °C in 5 min and heating from 10 °C to the set measurement temperature in 5 min
(6) isothermal treatment for 5 min at the set measurement temperature.

Steps #1 and #2 were repeated at least three times. As soon as the coagel turned into the gel phase, the vial was put in a refrigerator at 4 °C for the reverse transition to occur. The procedure was repeated at least five times until no air bubble

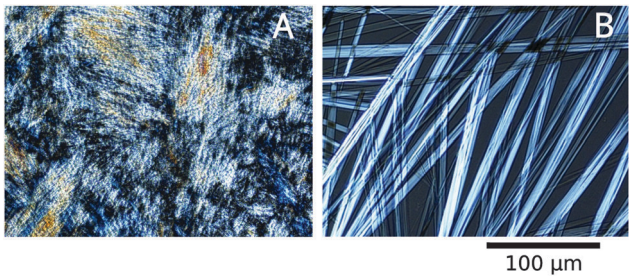

Fig. 3 Optical micrographs of an aqueous dispersion of L-ASC12, $w_{\text{L-ASC12}}$ = 30%. The images were collected before (A) and after (B) the annealing at 65 °C.

could be detected by visual inspection. The specimen was then sealed and stored in the refrigerator for the following experiment.

The efficacy of this method was verified through optical microscopy measurements. Fig. 3 shows two micrographs collected immediately after setting the coagel sample on the slide with a spatula (Fig. 3A) and after the annealing procedure carried out directly under the microscope (Fig. 3B). This procedure was used to verify that after the annealing cycle the coagel structure was intact. We recall that the pH of the medium where the surfactant is dispersed does not affect its phase behaviour, at least between pH 2 and 7.4, therefore we used pure double distilled Millipore water as the solvent.[4]

2.3 Rheology measurements

All rheology tests were performed using a Physica-Paar UDS 200 rheometer, equipped with a plate–plate geometry measuring system (diameter of the upper plate 2.5 cm, measuring gap: 1 mm). Temperature was controlled with a Peltier device.

All the oscillatory measurements were performed within the linear viscoelastic range. In order to minimise the evaporation of water, silicone oil was applied to the rim of the samples. The instrumental setups for the rheology tests are the following:

Frequency sweep test: frequency range 100 Hz to 0.001 Hz; amplitude 0.001%;

Flow curve: torque range 0.0 mN m^{-1} to 100 mN m^{-1};

Temperature test sweep: frequency 0.25 Hz, amplitude 0.1%, temperature 60 °C to 10 °C linear scale.

2.4 Optical microscopy

Inspections of coagel samples before and after shearing were conducted using a Nikon Diaphot 300 optical microscope equipped with a digital camera (Nikon Digital Sight DS-U1). The length of the crystals was measured by analysing the images with the software Inkscape 0.91.[11] The temperature of the sample was changed during the inspection using a Peltier device. The gel phases are isotropic, and no information could be obtained by observation under the microscope.

2.5 SAXS

SAXS measurements were carried out with a HECUS S3-MICRO camera (Kratky-type) equipped with a two position-sensitive detector (OED 50 M) containing 1024 channels of width 54 μm. CuK_α radiation (wavelength λ = 1.542 Å) was provided by an ultra-brilliant point micro-focus X-ray source (GENIX-Fox 3D, Xenocs, Grenoble), operating at a maximum power of 50 W (50 kV and 1 mA). The sample-to-detector distance was 281 mm. The volume between the sample and the detector was kept under vacuum during the measurements to minimize scattering from the air. The Kratky camera was calibrated in the small angle region using silver behenate (d = 58.34 Å),[12] while lupolen (d = 4.12 Å and 3.8 Å) was used as a reference for the wide-angle region. SAXS curves were obtained in the scattering vector (q) range between 0.01 Å^{-1} and 0.54 Å^{-1}, where $q = (4\pi/\lambda)\sin\theta$, 2θ being the scattering angle. The WAXS region covered in the experiment was from 1.3 Å^{-1} to 1.9 Å^{-1}. Samples were placed into an open demountable cell (total sample thickness = 1 nm) using Nalophan® tape as windows. The temperature was set to 25 °C and controlled by a Peltier element, with an accuracy of ±0.1 °C. All scattering curves were corrected for the empty cell contribution considering the relative transmission factor.

2.5.1 Model for SAXS data fitting. The SAXS patterns in the gel state were fitted according to the approach proposed by Nallet *et al.*,[13] by using the SasView 3.0.0 package.[14] The total SAXS intensity, $I(q)$, was calculated taking into account the scattering length density of the C_{11} hydrocarbon tail region (ρ_{tail}), of the head group region (ρ_{head}), and of the solvent (ρ_{H_2O}) as well as the instrumental resolution of the SAXS apparatus (Δq) and the powder averaging. The scattering intensity is given by:

$$I(q) = A\frac{2\pi P(q)S(q)}{d_0 q^2} + \text{background} \quad (1)$$

where A is a prefactor that takes into account the volume fraction of the sample and the fact that the data were not converted in absolute units, d_0 is the lamellar repeat spacing, $P(q)$ is the form factor, $S(q)$ the structure factor and background is the background noise. Considering the scattering length density distribution inside the lamellae, the form factor can be expressed as:

$$P(q) = \frac{4}{q^2}\{\Delta\rho_{\text{H}}[\sin[q(\delta_{\text{H}} + \delta_{\text{T}})] - \sin(q\delta_{\text{T}})] + \Delta\rho_{\text{T}}\sin(q\delta_{\text{T}})\}^2 \quad (2)$$

where $\Delta\rho_{\text{H}}$ (or $\Delta\rho_{\text{T}}$) is the difference between the head group (or the tail) and solvent scattering length densities. δ_{H} and δ_{T} are the head group thickness and the length of the hydrocarbon tail, respectively. The description of the lamellar distribution is depicted in Fig. 4. An effective structure factor is combined with the form factor to take into account the modulation of the shape and the height of the Bragg peaks, the finite instrumental resolution and powder averaging proper of the sample:

$$S(q) = 1 + 2\sum_{1}^{N-1}\left(1 - \frac{n}{N}\right)\cos\left(\frac{qd_0 n}{1 + 2\Delta q^2 d_0^2 \alpha(n)}\right) \times \exp\left(\frac{2q^2 d_0^2 \alpha(n) + \Delta q^2 d_0^2 n^2}{2 + 4\Delta q^2 d_0^2 \alpha(n)}\right)\frac{1}{\sqrt{1 + 2\Delta q^2 d_0^2 \alpha(n)}} \quad (3)$$

N is an integer number representing the number of lamellar plates, Δq is the width of the instrumental resolution function as experimentally determined by the measurement of the direct

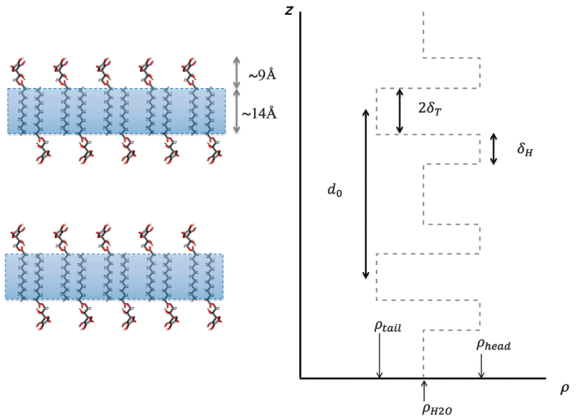

Fig. 4 Schematic representation of the geometrical lamellar arrangement (left) and the corresponding X-ray scattering length profile (right).

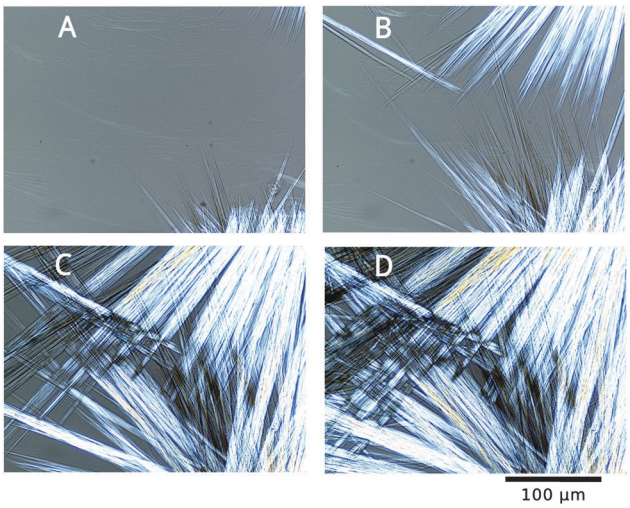

Fig. 5 Optical micrographs on a L-ASC12 aqueous dispersion, $w_{\text{L-ASC12}}$ = 20%. The micrographs (from A to D) were collected 5 s, 20 s, 40 s and 60 s after the cooling of the gel from 55 °C to 40 °C.

X-ray beam. $\alpha(n)$ is the correlation function for the lamellae that directly depends on the Caillé parameter, η_{cp}:

$$\alpha(n) = \frac{\eta_{\text{cp}}}{4\pi^2}[\ln(\pi n) + \gamma_{\text{E}}] \quad (4)$$

$$\eta_{\text{cp}} = \frac{q_0^2 k_{\text{B}} T}{8\pi\sqrt{K\bar{B}}} \quad (5)$$

where γ_{E} is the Euler's constant, K is the smectic bending elasticity, $\bar{B}$ is the compression modulus, q_0 is the position of the first-order Bragg peak, k_{B} the Boltzmann constant, and T the absolute temperature of the sample.

Due to the large number of parameters in eqn (1), some of them must be pre-determined and fixed during the fitting procedure. In particular, the lamellar spacing can be directly extracted from the first-order Bragg-peak position as $d_0 = 2\pi/q_0$, Δq can be measured from the direct beam shape (0.00245 Å^{-1}), and ρ_{tail} and $\rho_{\text{H}_2\text{O}}$ are calculated from the chemical formula and densities of undecane and water using the SLD calculator tool available in SasView 3.0.0 (at 20 °C $\rho_{\text{tail}} = 7.2 \times 10^{-6}$ Å^{-2} and $\rho_{\text{H}_2\text{O}} = 9.4 \times 10^{-6}$ Å^{-2}).[14] Their temperature dependence was taken into account, although it is marginal. Moreover, a fixed value of 50 was chosen for N since a negligible change of the scattering intensity was found for values bigger than 30 (*i.e.* the N value cannot be determined by the SAXS experiment). Therefore there were only six free fitting parameters left: the prefactor A, the background, the tail and head contributions to the membrane thickness, $\delta = \delta_{\text{H}} + \delta_{\text{T}}$, the Caillé parameter, η_{cp} and the scattering length density of the head group, ρ_{head}. The fittings were performed using the SasView program version 3.0.0.[14]

3 Results and discussion

3.1 Microscopy and growth of the coagel

Fig. 5 shows a sequence of crossed-Nicols optical micrographs of the L-ASC12 system ($w_{\text{L-ASC12}}$ = 20%) undergoing the phase transition from gel back to coagel, after the annealing procedure described in Section 2.2. The sequence shows the progressive formation of a 3D network with an interconnected lamellar structure built by the aggregation of fibrillar crystals with dimensions in the order of a few microns.

The growth of the coagel crystals occurs in one direction and the length of the crystals can be directly monitored from the optical micrographs collected at fixed time intervals (Fig. 6). Then, by measuring the variation of the length of the needle-shaped crystals, we obtained the degree of advancement of the reaction ξ, that describes the growth of the network structure as a function of time:

$$\xi = \frac{l(t) - l(0)}{l(\infty) - l(0)} \quad (6)$$

where $l(t)$ is the length of the crystal at time t, $l(0)$ is the initial length of the crystal and $l(\infty)$ is the length of the crystal at the end of growth.

The phenomenological Avrami-Erofee'v model (see eqn (7))[15,16] describes the kinetics of a crystallisation process at constant temperature:

$$\xi = 1 - \exp(-kt^M) \quad (7)$$

where k is the rate constant and M is the exponent associated to the nucleation type and related to the dimensionality of the product phase, type of growth, and nucleation rate. In particular, M is related to the mechanism of the reaction through the coefficients P, Q, and S, according to the following equation:

$$M = \frac{P}{S} + Q \quad (8)$$

where P = 1, 2, or 3 corresponds to fibers, sheets, or polygonal forms growth, respectively; S = 1 or 2 indicates phase boundary growth or diffusion of the component through a liquid phase, respectively. Finally, Q = 0 or 1 means no nucleation, or constant nucleation.[17,18]

Fig. S1 in the ESI,† shows the results of the linear least-squares fitting of the plot $\ln[1 - \ln(1 - \xi(t))]$ *versus* $\ln(t)$ that

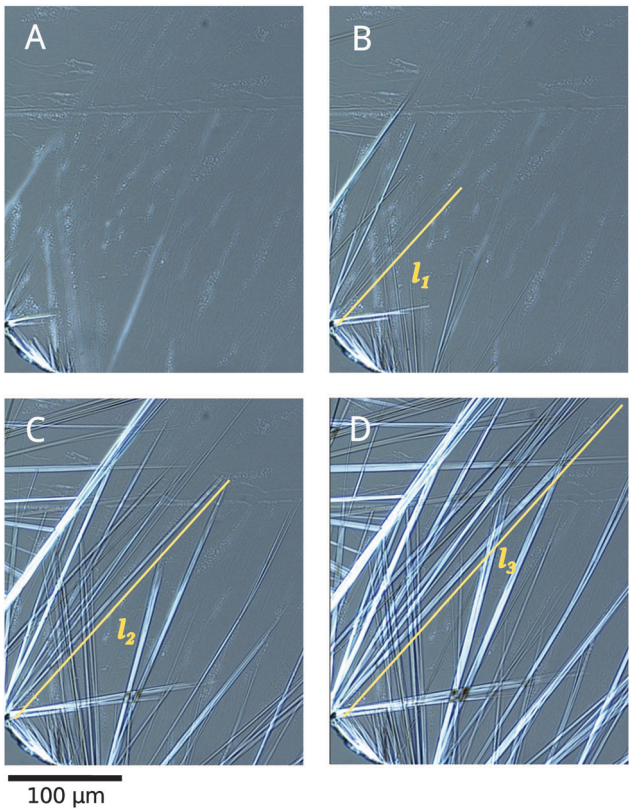

Fig. 6 Optical micrographs of the $w_{\text{L-ASC12}}$ = 20% system at different times (from A to D: 2 s, 9 s, 15 s, 21 s) after the cooling of the gel from 55 °C to 40 °C. The yellow line indicates one of the needle-shaped crystals used for the kinetics study. Its dimensions as measured on the computer screen are: l_1 = 160 μm, l_2 = 260 μm, l_3 = 370 μm.

gives the kinetic parameters k (from the intercept) and M (from the slope). This relationship fits very well the experimental data. The average values obtained by following the growth of many crystals, are equal to 1.57 ± 0.04 and (2.43 ± 0.01) × 10^{-2} respectively. As suggested by the micrographs in Fig. 5 and 6, the crystals grow unidirectionally, therefore we set P equal to unity. Hence the only possible values for S and Q are 2 and 1, respectively. This set of (P, S, Q) values corresponds to a process driven by the diffusion of the gelator molecules into the liquid phase to the interface (S = 2), occurring at constant nucleation (Q = 1).

3.2 SAXS

Fig. 7 shows the SAXS pattern associated to a $w_{\text{L-ASC12}}$ = 10% sample as the temperature is increased from 20 °C to 65 °C, across the coagel to gel transition temperature, which is around 46 °C to 47 °C.

When the temperature is below 50 °C the SAXS patterns reveal a prominent peak around 0.164 Å^{-1}. This feature is associated to a lamellar arrangement of the hydrated solid with a total lattice spacing $d_0 = 2\pi/q_0$ = 6.28/0.164 Å ≈ 38.1 Å. The extracted thickness is in agreement with an interdigitated, non-tilted packing of the hydrophobic chains as we found in previous studies.[19]

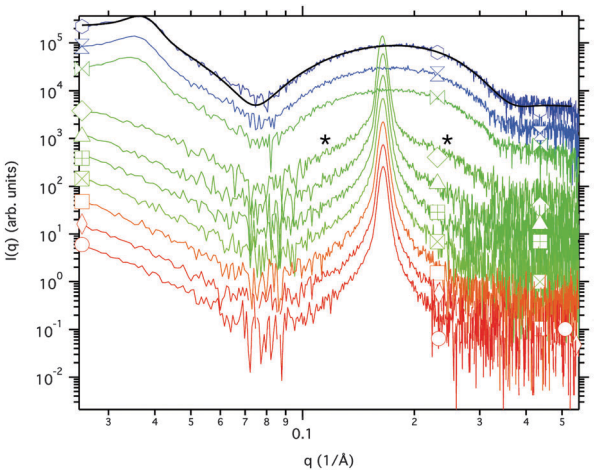

Fig. 7 Log–log representation of the SAXS scattering intensity distribution for a $w_{\text{L-ASC12}}$ = 10% L-ASC12/water sample at: 20 °C (○), 25 °C (◊), 30 °C (□), 35 °C (⊠), 40 °C (⊞), 45 °C (△), 50 °C (◇), 55 °C (⋈), 60 °C (⧖), 65 °C (⬡). The black continuous line is an example of the fitting results in the case of the gel state at 65 °C. The asterisks evidence that at 50 °C the coagel and the gel coexist. Curves are arbitrarily shifted on the y-axis for the sake of clarity.

A temperature increment above 50 °C results in a shift of the first order reflection towards lower q values and in a significant broadening of the peak. The peak at 0.164 Å^{-1} is replaced by a broad hump. All these changes indicate an increment in the amount of water confined in the hydration layer and thus a swelling of the lamellar structure. Remarkably, at 50 °C the coexistence of both the coagel and gel phases is shown by the presence of both the Bragg peak at 0.164 Å due to the coagel, and of the broad peak due to the gel phase (see also Fig. S2 in the ESI†). The SAXS patterns were modeled according to the approach proposed by Nallet *et al.*[13] (see Section 3.2), and the extracted parameters are listed in Table 1.

The model fits the SAXS curves for the gel state in the entire q-range of the experiment. Hence, the gel structure is a result of an anisotropic expansion of the tightly packed coagel, and can be depicted as a set of swollen lamellae where extra water is uptaken in the inter-lamellar region. In the case of the $w_{\text{L-ASC12}}$ = 10% sample the total lamellar spacing increases from 38 Å to about 170 Å as temperature increases. The parameters δ_H and δ_T are about 12 Å and 7 Å respectively. The transition brings about also a dramatic increment in the thermal fluctuations of the system as the Caillé parameter raises from 0.08 to about 0.7 (a Caillé parameter equals to zero means no thermal fluctuation).[20] This result points out that the thickness of the hydrophilic layer increases slightly from 10 Å to 12 Å, with a small increment in the number of water molecules that solvate the head groups. However the most striking consequence is the significant reduction in the hydrophobic layer thickness, from 18 Å to 7 Å. This is in line with the description of the gel state with molten, tilted and loosened alkyl chains in the lipophilic portion. The very large hydrophilic pool then includes intermediate water molecules, where the term intermediate refers to their dynamic properties: in fact these molecules are neither restrained in their freedom of motion as

Table 1 Fitting parameters for selected curves throughout the temperature series for the $w_{\text{L-ASC12}}$ = 10% and $w_{\text{L-ASC12}}$ = 35% L-ASC12/water samples

$w_{\text{L-ASC12}}$	T/°C	η_{cp}	δ_H/Å	δ_T/Å	ρ_{head}/1/Å^2	d_0/Å	Background
10%	25[a]	0.08(3)[b]	—	—	—	38.1(5)	—
	35[a]	0.08(3)[b]	—	—	—	38.2(5)	—
	45[a]	0.08(3)[b]	—	—	—	38.3(6)	—
	55	0.686(8)	12.4(2)	6.7(1)	$1.14(6) \times 10^{-5}$	177(1)	0.231(4)
	60	0.676(8)	11.8(2)	6.9(1)	$1.14(6) \times 10^{-5}$	175(1)	0.232(4)
	65	0.700(8)	11.8(2)	6.8(1)	$1.15(6) \times 10^{-5}$	169(1)	0.239(4)
35%	25	0.02(3)[b]	—	—	$1.13(6) \times 10^{-5}$	38.0(5)	—
	65	0.55(9)	10.2(4)	7.6(3)	$1.15(6) \times 10^{-5}$	61.7(8)	0.213(5)

[a] Due to the presence of one reflection order in the coagel state only the total lattice spacing could be obtained. [b] Estimated from the fitting of the Bragg peak at 0.164 Å^{-1} and fixing all the other parameters.

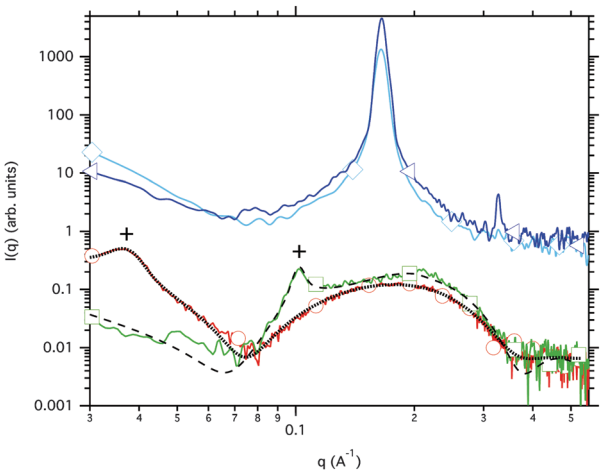

Fig. 8 Log–log representation of the SAXS scattering intensity distribution for two L-ASC12/water samples: $w_{\text{L-ASC12}}$ = 10% at 25 °C (◇) and at 65 °C (○); $w_{\text{L-ASC12}}$ = 35% at 25 °C (◁) and at 65 °C (□). Black dashed lines are the fitting results for the correspondent gel states at 65 °C. The (+) symbols mark the shift of the first reflection order in the gel state as the mass fraction is increased from 10% to 35%. Curves are arbitrarily shifted on the y-axis for the sake of clarity.

strongly bound interfacial water, nor free to move as water in its standard liquid state at the same temperature.[3]

Fig. 8 reports the SAXS curves before and after the coagel-to-gel transition for the $w_{\text{L-ASC12}}$ = 10% and the $w_{\text{L-ASC12}}$ = 35% samples for comparison. The fitting parameters obtained for the fitting of the coagel state at $w_{\text{L-ASC12}}$ = 35% are listed in Table 1. The curves before the transition (dark blue and light blue curves) show no difference in the coagel state and the lamellar spacing is about 38 Å. After the transition (red and green curves), the swollen lamellae in the two samples show very different spacing, passing from 170 Å for the $w_{\text{L-ASC12}}$ = 10% sample to about 62 Å for the $w_{\text{L-ASC12}}$ = 35% specimen. The thermal fluctuations are reduced both in the coagel and in the gel state as a consequence of the mass fraction increment.

3.3 Rheology

In order to investigate the effect of the temperature on the viscosity of both gels and coagels, we collected several flow curves on a $w_{\text{L-ASC12}}$ = 30% L-ASC12/water sample at different temperatures, below and above the coagel-to-gel transition temperature (see Fig. S3 in the ESI†). The Arrhenius model was used to determine the flow activation energy:

$$\eta_0 = A \exp\left(\frac{E_a}{RT}\right) \quad (9)$$

where η_0, A, E_a, R and T are the zero shear stress viscosity (in Pa s), the pre-exponential factor (in Pa s), the flow activation energy (in J mol^{-1}), the gas constant (8.31 J K^{-1} mol^{-1}) and the absolute temperature (in K), respectively. The temperature ranges for the evaluation of the activation energies were determined by the thermal stability of the two phases and of the L-ASC12 that decomposes around 65 °C. The activation energy obtained from the Arrhenius plot decreases from (120 + 10) kJ mol^{-1} for the coagel to (23 + 4) kJ mol^{-1} for the gel. This change is due to the different structure of the gel. In fact, as suggested by the values listed in Table 1, the gel possesses a less compact structure than the coagel, as the increment of the interlayer distance d_0 and of the bilayer flexibility expressed by the Caillé parameter η_{cp} clearly indicate. In passing we note that the value of E_a for the L-ASC12/water gel is comparable to that obtained with primary amines in silicone oil.[21]

Dynamic mechanical measurements were performed to explore the viscoelastic properties of the gels produced by L-ascorbyl-dodecanoate. Fig. S4 in the ESI,† shows the storage (G') and the loss component (G'') of the complex modulus (G^*) as a function of frequency ω at different L-ASC12 mass fractions. For all samples G' is always larger than G'' in the investigated range of frequencies, without a crossover point between the shear moduli, a behavior that is typical of a gel system. Moreover, G' and G'' are almost independent on the frequency. This result also indicates that the physical junctions in the network behave as permanent cross-links with long lifetimes, a behaviour that is typical of other self-assembled systems.[22]

This behaviour shows that when the densely packed lamellar phase (the coagel) collapses upon heating, the sample behaves as a common gel according to the definition given by Almdal *et al.*:[23] a gel is a solid or semi solid material which consists of at least two components, one of which is a liquid and that is soft and resilient. The latter property means that the mechanical damping in the material is small, *i.e.* $\tan\delta = G''(\omega)/G'(\omega) \ll 1$ in the relevant frequency range, $G'(\omega)$ being the storage shear modulus and $G''(\omega)$ the loss shear modulus.

Fig. S5 in the ESI,† shows that the trend of the elastic modulus G' at 0.5 Hz as a function of the surfactant concentration suggests two different regimes: for L-ASC12 mass fractions below 30% the G'(0.5 Hz) values are almost constant, while above this value the slope increases dramatically. More work is necessary to fully describe and understand the nature of such concentration limit.

Oscillatory temperature tests were performed in order to reproduce the coagel-to-gel transition temperature (T_t) under oscillating stress. Fig. 9 shows the trend of the T_t values as a function of the L-ASC12 mass fraction. The coagel-to-gel transition temperatures, T_t were taken at the onset of the slope variation. Two different regimes can be identified: for L-ASC12 mass fractions ranging below 25%, the T_t value remains almost constant, between 40.5 °C and 42 °C; for higher mass fractions, T_t values increase up to approximately 45 °C for the $w_{\text{L-ASC12}}$ = 35% sample. These values are significantly smaller than those obtained through DSC reported in previous papers,[4,24] due to the applied oscillating perturbation that promotes the coagel-to-gel transition.

The data reported in Fig. 9 and Fig. S5 in the ESI,† indicate that once the L-ASC12 mass fraction reaches a value between 25% and 30%, a structural transition with a rapid increase of the strength of the network takes place. This is also confirmed by the SAXS data. As a matter of fact Table 1 suggests that upon increasing the L-ASC12 mass fraction from 10% to 35% for gel systems a significant decrease of both d_0 (from 170 Å to 62 Å) and η_{cp} (from 0.7 to 0.55) occurs. This effect may reflect the depletion of a substantial amount of water from the interlamellar region, due to the mechanical stress imparted by the oscillating plates.

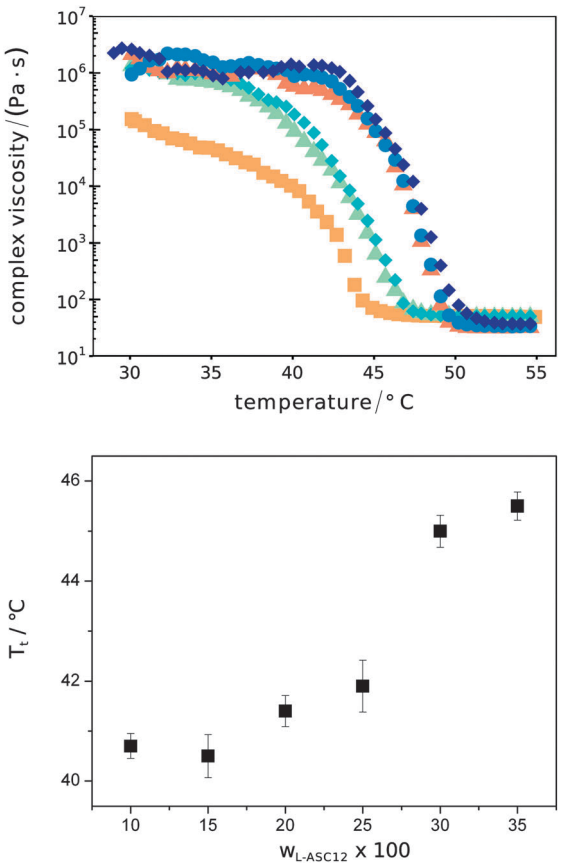

Fig. 9 Top: Complex viscosity η^* of L-ASC12/water dispersions as a function of temperature. The curves correspond to L-ASC12/water systems with a surfactant mass fraction of: 10% (■), 15% (▲), 20% (◆), 25% (▲), 30% (●), 35% (◆). Bottom: Coagel-to-gel transition temperature as a function of the L-ASC12 mass fraction in the sample, obtained from the plot on the left.

Interestingly this phenomenon can be depicted as a partial transition from the gel to the coagel state, due to a concentration increment rather than to a cooling process.

The dependence of the G' modulus (measured at a frequency of 1 Hz) on the solute concentration for various systems at different viscosities is discussed in the literature in terms of a power law.[25] Fig. S6 (ESI†) shows the plot of G' *versus* the surfactant mass fraction in the logarithm scale. The data are well fitted by a linear regression with a slope of n = 2. According to the theory describing the behaviour of polymers in solution, this value suggests that the expansion of the L-ASC12 based network occurs through a percolation mechanism.[26]

Finally, according to the Jones–Marques theory we can calculate the fractal dimension of the rheological units, D_F: $(3 + D_F)/(3 - D_F) = n$. In our case n = 2 and therefore D_F = 1. This result confirms what we already concluded from the optical microscopy observations (see Fig. 5 and 6) and from the Avrami fitting, *i.e.* that the system comprises monodimensional fibrils.

3.4 Thermodynamic analysis

The coagel-to-gel phase transition is associated to a measured enthalpy change ΔH_{trans} that is usually described in terms of three contributions: the conformational and packing change of the alkyl chains (ΔH_{chain}), the release of the acidic proton (ΔH_{el}) and the hydration of the polar heads (ΔH_{hydr}):[27]

$$\Delta H_{trans} = \Delta H_{chain} + \Delta H_{el} + \Delta H_{hydr} \quad (10)$$

The first two terms are endothermic while the latter is exothermic.[24] In the literature, ΔH_{chain} is usually related to a partial melting of the hydrophobic tails but without any other more precise evaluation of the molten state of the chains in the gel state.

In order to quantify the degree of fusion of the aliphatic chains during the coagel-to-gel phase transition we approximate the sum $\Delta H_{el} + \Delta H_{hydr}$, *i.e.* the overall enthalpic change related to all interactions between the surfactant's head groups and the surrounding aqueous medium, to the enthalpy of solvation of an L-ascorbic acid molecule, ΔH_{solv}, that can be estimated as:

$$\Delta H_{solv} = \Delta H_{sol} - \Delta H_{latt} \quad (11)$$

Here ΔH_{sol} is the solution enthalpy and ΔH_{latt} is the lattice enthalpy for L-ascorbic acid. The values of ΔH_{sol} and of ΔH_{latt} were taken from the literature and are about 23 kJ mol^{-1} [28] and 25 kJ mol^{-1},[29] respectively, from which we obtain $\Delta H_{solv} \approx -2$ kJ mol^{-1}.

The enthalpy change of melting ΔH_m for pure L-ASC12 is 39 kJ mol^{-1} [4] and the measured enthalpy change for the coagel-to-gel phase transition in a $w_{\text{L-ASC12}}$ = 10% sample is

ΔH_{trans} = 37 kJ mol^{-1}.[24] If β indicates the percentage fraction of alkyl chains that melt during the coagel-to-gel phase transition, we have:

$$\Delta H_{trans} = \beta \Delta H_m + \Delta H_{solv} \quad (12)$$

and substituting the given values we calculate that β is roughly equal to 1.

This result suggests that during the phase transition the dodecyl chains melt almost completely, and that in the gel state the alkyl chains are in a liquid-like state, as in the core of a micellar aggregate.[1]

In this simple description we do not disregard the fact that the solvation enthalpy of the ascorbic acid heads is probably lower than that of pure ascorbic acid molecules in water, because the pK_a of the hydrophilic heads in the nanostructure is certainly greater than that of L-ascorbic acid in solution (3.36),[7,30] and because water molecules cannot freely interact with the polar heads as they solvate an L-ascorbic acid moiety in a molecular solution. However, the main role in the entire coagel-to-gel transition is certainly played by the aliphatic chains rather than by the head groups. In fact it is interesting to compare the enthalpy change of melting of different compounds that bear a dodecyl chain: for dodecane ΔH_m is 35.7 kJ mol^{-1},[31] that of 1-dodecanol is 40.3 kJ mol^{-1},[32] and that of dodecanoic acid is 36.1 kJ mol^{-1},[33] suggesting that the conformational and packing changes of the hydrophobic portions in these different compounds play the major effect.

4 Conclusions

We investigated the structural features of coagels and gels produced by L-ascorbyl-dodecanoate (L-ASC12) in water by SAXS and rheology tests.

The results indicate that the formation of the gel phase brings about the collapse of the densely packed lamellar structure, with a melting of the alkyl chains, a significant reduction of the hydrophobic layer thickness, and a dramatic expansion of the interlamellar water compartment. As a result of the loosened structure, the thermal fluctuations in the gel state increase, as suggested by the Caillé parameter η_{cp} extracted from the SAXS profiles. Upon cooling, the more ordered coagel state is promptly reformed, with a narrower hydrophilic pool that contains only strongly bound water molecules around the polar head groups of the surfactants.

Rheology tests on the coagel and gel states confirm the less compact structure in the latter, as suggested by the reduced value of the activation energy. Dynamic mechanical experiments reveal the presence of a mass fraction value at about 30%, a threshold due to the onset of stronger interactions between the rheological units. Interestingly, SAXS and rheology experiments indicate that the increment in the L-ASC12 mass fraction from 10% to 35% for a gel system results in consistent lowering of both the lamellar spacing d_0 and of η_{cp}. We argue that such phenomenon is due to the depletion of water from the interlamellar region, imparted by the mechanical stress.

In conclusion, during the coagel-to-gel phase transition the hydrocarbon chains melt completely and acquire the conformational freedom typical of a liquid state, as in a micellar core. As a result, the hydrophobic layer in the gel becomes thinner and more disordered, resulting in turn in a greater distance between the surfactant's monomers. The ascorbic acid head groups release the proton, and get solvated by the water molecules. Since a net negative charge appears on the lamellar interface after the deprotonation of the head groups, the surfactants' bilayers are subject to a strong electrostatic repulsion and the intermediate water pool becomes much wider.

Acknowledgements

The authors acknowledge CSGI and the Enzo Ferroni Foundation for partial financial support and for helpful discussions.

References

1 B. W. Ninham and P. Lo Nostro, *Molecular forces and self assembly: in colloid, nano sciences and biology*, Cambridge University Press, 2010.
2 M. Ambrosi, E. Fratini, V. Alfredsson, B. Ninham, R. Giorgi, P. Lo Nostro and P. Baglioni, *J. Am. Chem. Soc.*, 2006, **128**, 7209–7214.
3 S. Borsacchi, M. Ambrosi, P. Lo Nostro and M. Geppi, *J. Phys. Chem. B*, 2010, **114**, 15872–15878.
4 P. Lo Nostro, B. W. Ninham, M. Ambrosi, L. Fratoni, S. Palma, D. Allemandi and P. Baglioni, *Langmuir*, 2003, **19**, 9583–9591.
5 M. Ambrosi, P. Lo Nostro, L. Fratoni, L. Dei, B. W. Ninham, S. Palma, R. H. Manzo, D. Allemandi and P. Baglioni, *Phys. Chem. Chem. Phys.*, 2004, **6**, 1401–1407.
6 P. Lo Nostro, R. Ramsch, E. Fratini, M. Lagi, F. Ridi, E. Carretti, M. Ambrosi, B. W. Ninham and P. Baglioni, *J. Phys. Chem. B*, 2007, **111**, 11714–11721.
7 M. Ambrosi, P. Lo Nostro, E. Fratini, L. Giustini, B. W. Ninham and P. Baglioni, *J. Phys. Chem. B*, 2009, **113**, 1404–1412.
8 P. Lo Nostro, M. Ambrosi, B. W. Ninham and P. Baglioni, *J. Phys. Chem. B*, 2009, **113**, 8324–8331.
9 M. Kodama and S. Seki, *Adv. Colloid Interface Sci.*, 1991, **35**, 1–30.
10 G. Capuzzi, P. Lo Nostro, K. Kulkarni and J. E. Fernandez, *Langmuir*, 1996, **12**, 3957–3963.
11 *Inkscape 0.91*, https://inkscape.org/en/, last accessed: Feb 14, 2016.
12 T. N. Blanton, M. Rajeswaran, P. W. Stephens, D. R. Whitcomb, S. T. Misture and J. A. Kaduk, *Powder Diffr.*, 2011, **26**, 313–320.
13 F. Nallet, R. Laversanne and D. Roux, *J. Phys. II*, 1993, **3**, 487–502.
14 *SasView*, http://www.sasview.org/, last accessed: Oct 7, 2015.
15 M. Avrami, *J. Chem. Phys.*, 1940, **8**, 212–224.
16 M. Avrami, *J. Chem. Phys.*, 1941, **9**, 177–184.

17 R. Berliner, M. Popovici, K. Herwig, M. Berliner, H. Jennings and J. Thomas, *Cem. Concr. Res.*, 1998, **28**, 231–243.
18 P. Lo Nostro, L. Giustini, E. Fratini, B. W. Ninham, F. Ridi and P. Baglioni, *J. Phys. Chem. B*, 2008, **112**, 1071–1081.
19 C. Venturini, C. Pomposi, M. Ambrosi, E. Carretti, E. Fratini, P. Lo Nostro and P. Baglioni, *J. Phys. Chem. B*, 2014, **118**, 3053–3062.
20 M. Kléman and O. D. Laverntovich, *Soft matter physics: an introduction*, Springer-Verlag, New York, 2003.
21 E. Carretti, M. George and R. G. Weiss, *Beilstein J. Org. Chem.*, 2010, **6**, 984–991.
22 S. Hyde, B. Ninham and T. Zemb, *J. Phys. Chem.*, 1989, **93**, 1464–1471.
23 K. Almdal, J. Dyre, S. Hvidt and O. Kramer, *Polym. Gels Networks*, 1993, **1**, 5–17.
24 S. Palma, R. H. Manzo, D. Allemandi, L. Fratoni and P. Lo Nostro, *Langmuir*, 2002, **18**, 9219–9224.
25 P.-G. De Gennes, *Scaling concepts in polymer physics*, Cornell university press, 1979.
26 M. Pääkkö, M. Ankerfors, H. Kosonen, A. Nykänen, S. Ahola, M. Österberg, J. Ruokolainen, J. Laine, P. T. Larsson and O. Ikkala, *et al.*, *Biomacromolecules*, 2007, **8**, 1934–1941.
27 P. Lo Nostro, B. W. Ninham, L. Fratoni, S. Palma, R. H. Manzo, D. Allemandi and P. Baglioni, *Langmuir*, 2003, **19**, 3222–3228.
28 A. Shalmashi and A. Eliassi, *J. Chem. Eng. Data*, 2008, **53**, 1332–1334.
29 A. Arslantas, W. C. Ermler, R. Yazici and D. M. Kalyon, *Int. J. Mol. Sci.*, 2005, **6**, 291–302.
30 J. Kanicky and D. Shah, *Langmuir*, 2003, **19**, 2034–2038.
31 D. Mondieig, F. Rajabalee, V. Metivaud, H. Oonk and M. Cuevas-Diarte, *Chem. Mater.*, 2004, **16**, 786–798.
32 J. C. van Miltenburg, G. J. van den Berg and M. Ramirez, *J. Chem. Eng. Data*, 2003, **48**, 36–43.
33 E. Moreno, R. Cordobilla, T. Calvet, M. Cuevas-Diarte, G. Gbabode, P. Negrier, D. Mondieig and H. A. Oonk, *New J. Chem.*, 2007, **31**, 947–957.